Sinkhole Monitoring and Early Warning Detection in the Karst Landscapes of Guimaras Island, Philippines Using Interferometric Synthetic Aperture Radar (InSAR) Satellite Data

Laurelly Joyce A. Aporto[1], Luis Carlo S. Mabaquiao[2], Leonardo Miguel Garcia[1], Pia Franchesca R. Maralit[1], Mario Jr. G. Ugalino[1], Kim Elijah M. Aguilan[1], Jarence David D. Casisirano[1], Albert Francis P. Florin[1], Karlo Mark C. Tablang[1], Fatima Joy O. Pamittan[1], Dominic Jr. C. Fargas[1], Czar Jakiri S. Sarmiento[1,2]

[1]Training Center for Applied Geodesy and Photogrammetry, University of the Philippines Diliman, Quezon City, Philippines – (laaporto1, lgarcia1, prmaralit, mgugalino1, kmaguilan, jdcasisirano, apflorin, kctablang, fopamittan, dcfargas, cssarmiento)@up.edu.ph

[2]Department of Geodetic Engineering, University of the Philippines Diliman, Quezon City, Philippines – lsmabaquiao@up.edu.ph

Keywords: InSAR, Persistent Scatterer Interferometry, DRRM, Sinkholes, Karst subsidence.

Abstract

Guimaras Island in the Philippines is underlain by karst landscapes that pose a risk of ground subsidence and potential sinkhole formation, particularly in the municipalities of Buenavista, Jordan, and Nueva Valencia. This study explores the use of Interferometric Synthetic Aperture Radar (InSAR), specifically the Persistent Scatterer Interferometry (PSI) technique, to monitor ground displacement and identify early signs of karst-related subsidence. Sentinel-1 data from 2024 to 2025 was processed using the StaMPS workflow, generating 26,529 persistent scatterer (PS) points primarily over built-up and urban areas. A total of 3,807 subsiding scatterers were identified, with mean vertical displacement velocities reaching up to –36 mm/year in Nueva Valencia. Bivariate Ripley's K-function analysis revealed that subsiding PS points deviate from spatial randomness, but they exhibit negative spatial association with known sinkhole locations. This is attributed to the limitations of PSI, as a huge amount of points in the sinkhole inventory are located in vegetated areas where persistent scatterers are sparse which limits PSI coherence and detection capability. This emphasizes the need for ground validation to effectively detect and distinguish sinkhole hazards from other subsidence-related events in the study area. Through DBSCAN clustering analysis, areas with high localized subsidence were observed near infrastructure such as schools, barangay halls, and coastal residential areas. Generally, while the findings exhibited limitations in sinkhole detection capabilities of PSI, the methods were effective in detecting signs of localized subsidence in built-up areas in Guimaras. This provides a foundation for developing early warning and risk mitigation strategies against subsidence-related hazards in the area.

1. Introduction

1.1 Land Subsidence

The impact of geohazards on the environmental well-being, social fabric, and economic status of communities cannot be understated. Recent rise in anthropogenic activities and extreme weather events due to climate change have exacerbated these risks in many parts of the world over the past few decades (Peng & Tan, 2023). Geohazards, such as sinkholes and land subsidence, are especially considered to be extreme hazards not just because of the geographic extent of its destruction, but also because of the large amounts of uncertainties and unpredictability they possess (Nam et al., 2023).

Land subsidence is considered as a worldwide environmental, geological, and global issue (Bagheri-Gavkosh et al., 2021). It is characterized by the gradual sinking of the ground surface, resulting in a decrease in elevation relative to surrounding areas. Subsidence can be due to a variety of geological processes and factors, including increasing effective stress, sediment compaction, erosion, fluid withdrawal, and fault slipping (Galloway & Burbey, 2011). In the Philippines, land subsidence is revealed to be a major problem especially in urban and metropolitan areas such as the Province of Bulacan, Cebu, Davao, Iloilo, and Legazpi City, with subsidence rates going up to 109 millimeters per year (Sulapas et al., 2020).

1.2 Sinkholes

While land subsidence poses a threat to buildings and infrastructure, the associated surface deformation typically occurs gradually, allowing time for warnings to be issued and making catastrophic events less likely (Richardson, 2013). Sinkholes, on the other hand, typically occur with a sudden collapse. In areas underlain by karst landscapes, sinkholes can suddenly form, posing a significant threat to human settlements and infrastructure, particularly when triggered by factors such as heavy rainfall or seismic events. Such is the case with the October 2013 Bohol earthquake, where more than one hundred sinkholes were discovered in the aftermath of the disaster (Matus, 2013). The presence of sinkholes is generally not an immediate cause of concern; but extensive damage and loss of lives are expected if human settlements and infrastructures are built unknowingly on top of hidden sinkholes (Llanes et al., 2018).

Sinkholes generally occur suddenly and with little predictability; however, early warning signs such as tension cracks and ground subsidence often appear beforehand, which can develop gradually over months or even years before the area collapses. The presence of these precursory signs suggests the potential to identify early warning signals of sinkhole development before it fully collapses. Early detection of sinkholes by studying ground deformation and surface displacement can contribute to local communities for preventative measures, therefore reducing risk of injury and loss of life (Theron & Engelbrecht, 2018).

1.3 InSAR for Subsidence Monitoring

Monitoring ground subsidence has been done traditionally using devices such as Ground Penetrating Radar (GPR) and permanent GNSS stations. In the Philippines, monitoring subsidence hazards due to sinkholes fall within the jurisdiction of the Mines

and Geosciences Bureau (MGB) of the Department of Environment and Natural Resources (DENR) as part of their geohazard mapping and assessment efforts. The existing methodologies of DENR-MGB for generating sinkhole and susceptibility maps in karst areas include anecdotal accounts, geomorphological/geological assessment, and analysis of remote sensing data such as Digital Elevation Models and aerial photographs (MGB Region 6, 2018). While these methods generate data with high accuracy, significant gaps remain with regards to spatial resolution and coverage as well as resources and manpower allocation.

In recent years, the use of Interferometric Synthetic Aperture Radar (InSAR), a microwave remote sensing technique, to mitigate this gap has been on the rise as it has the capability to monitor ground deformation in large swaths and with reasonable accuracy. This is especially useful in areas with sparse GNSS stations. Research studies on subsidence around the world have utilized temporal InSAR to monitor ground deformation with high spatial and temporal resolution (Wu et al., 2022). InSAR measures ground deformation by analyzing the phase difference between two Synthetic Aperture Radar (SAR) images acquired over the same area at different times. This is observed along the satellite's line of sight (LOS) and enables the detection and measurement of ground displacement with sub-centimeter accuracy by deriving information from phase-change interferograms (Orhan, 2021).

Analysis of ground deformation using InSAR has two main categories of backscatter: Persistent Scatterers (PS) and Distributed Scatterers (DS). PS techniques, such as Persistent Scatterer Interferometry (PSI), are characterized by locating dominant scatterers (i.e. manmade structures, roads, rocks, poles) and are more effective in urban areas. On the other hand, DS techniques, such as Small BAseline Subset (SBAS), are effective in areas with sparse or random scatterers like vegetated or mountainous regions (Even et al., 2018).

InSAR-based ground deformation analysis to monitor sinkhole hazards or activities have been successfully applied to different study sites around the world. Susceptibility assessment and early warning detection specific to sinkhole hazards have been conducted on arid and vegetated areas (Kulshrestha, 2023; Orhan et al., 2023), as well as urbanized and suburban areas (Oliver-Cabrera et al., 2020; Malinowska et al., 2019).

Existing InSAR methodologies for sinkhole activity detection range from the use of deep learning techniques, mathematical and statistical modeling (Kulshrestha et al., 2021), Persistent Scatterer Interferometry (Oliver-Cabrera et al., 2020; Malinowska et al., 2019), and Small BAseline Subset (SBAS). Notably, between PSI and SBAS, PSI is more commonly utilized in sinkhole monitoring due to its precise nature. Time series PS deformation estimates typically have millimeter-level precision, allowing for the detection of very small ground deformations that may signal sinkhole activity (Malinowska et al., 2019).

1.4 Research Objectives

Studies on the use of remote sensing techniques such as InSAR to monitor ground subsidence in the Philippines have so far been focused on monitoring coastal subsidence (Ramirez et al, 2022) and subsidence in metropolitan areas (Sulapas et al., 2024). However, specific applications of InSAR deformation analysis for sinkhole monitoring and early detection have not been explored in local studies.

This study aims to explore the potential of Interferometric Synthetic Aperture Radar (InSAR) to identify, monitor, and detect sinkholes and early signs of karst subsidence in Guimaras. Specifically, this study aims:

1. To generate ground displacement velocity maps over the karst landscapes of Guimaras using Persistent Scatterer Interferometry (PSI) for high-resolution monitoring of surface deformation;
2. To assess spatial correlation characteristics between existing sinkhole inventory maps and PSI-derived results;
3. To detect and delineate areas of localized subsidence associated with potential sinkhole activity through clustering analysis of PSI-derived deformation data; and
4. To generate insights and recommendations for early warning systems for sinkhole hazards in karst environments using InSAR technologies.

The significance of this study lies not only in its potential to improve existing geohazard mapping techniques but also in its ability to provide early warning that can mitigate sinkhole risks. The highly accurate and high-coverage nature of PS-InSAR ground deformation monitoring make it a promising tool to augment existing sinkhole detection methods and maps in the Philippines. This is imperative in built-up areas underlain with karst topography, where existing MGB sinkhole maps may have blind spots due to noise and other urban characteristics. The findings of the study can serve as early warning detection for localized subsidence activities that are indicative of sinkhole events or karst processes, lessening risk to citizens and informing stakeholders before the hazard takes place.

2. Materials and Methods

2.1 Study Area

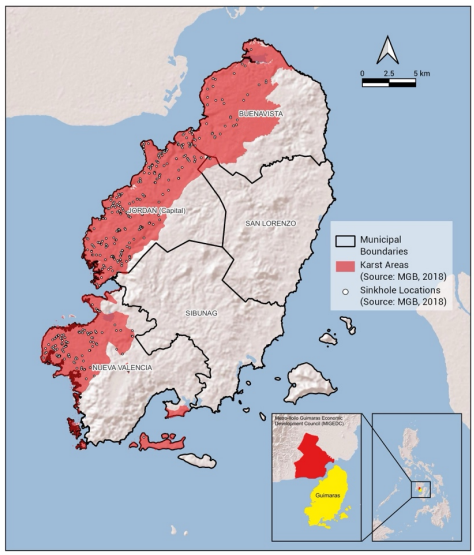

Figure 1. Province of Guimaras location map.

Guimaras is an island province located in the Western Visayas Region in the Philippines (Figure 1). It is composed of five coastal municipalities and has a land area of 60,547 hectares. The topography of the island is primarily steep, with ground elevation ranging from 0 to 300 meters above sea level (Province of Guimaras, 2019).

The province is known for its limestone formations, which make it particularly prone to sinkhole formation. The Guimaras

Provincial Development and Physical Framework Plan for 2020-2029 reports that priority concerns in Guimaras involve the presence of geological hazards where susceptibility to karst subsidence is a significant issue (IGES & PEMSEA, 2022).

According to the MGB, a total of 18,373.871 hectares in Guimaras have been identified as highly susceptible to karst subsidence. Of this total, the municipality of Jordan accounts for the largest share with 7,350.679 hectares, followed by Buenavista with 6,129.918 hectares, and Nueva Valencia with 4,893.274 hectares. Given that official karst subsidence hazard mapping by the MGB is a fairly new program (MGB Region 6, 2018), there is a possibility that karst subsidence in some areas in the island remain undetected.

2.2 Data Collection

2.2.1 Sinkhole Inventory: The MGB mapped the locations of sinkholes in the karst-prone municipalities of Jordan, Buenavista, and Nueva Valencia through a combination of anecdotal accounts, geomorphological/geological assessment, and IfSAR-DEM analysis. Within the three localities, a total of 433 sinkhole location points were determined — 36 in Buenavista, 267 in Jordan, and 130 in Nueva Valencia. Figure 1 shows the location of the sinkhole points in the sinkhole inventory. Notably, a large amount of sinkhole points lie within forested or vegetated areas of Guimaras.

2.2.2 SAR Satellite Images: The study utilized Synthetic Aperture Radar (SAR) images acquired in C-band (wavelength of 5.6 cm) and vertical co-polarization (VV) by the Sentinel-1A and 1B twin satellites via the Interferometric Wide (IW) beam mode. Each SAR image has an area coverage of about 250 km by 200 km, with a spatial resolution of 10 meters. For the study area, a total of 31 images (descending orbit, track 134) covering the period from March 7, 2024 to March 26, 2025 were obtained from the Alaska Satellite Facility (ASF) Data Search Portal.

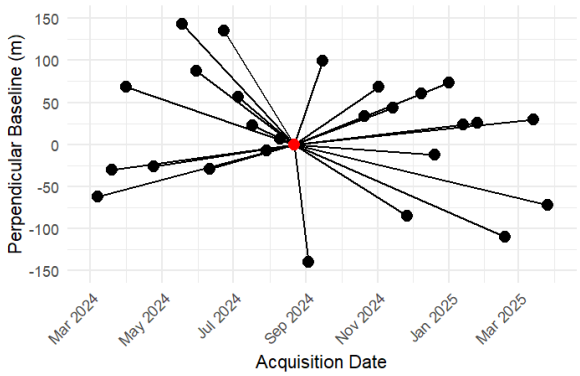

Figure 2. Perpendicular and temporal baselines of interferometric pairs. The red point represents the master image, the black points represent the slave images, and the lines represent the interferometric pairs.

Selecting the master image entails the minimizing of distribution of perpendicular baseline values, depicted in Figure 2, while maximizing the coherence across the interferometric stack. Selecting a suitable master image deals with the decorrelation effect, a loss of correlation between radar signals acquired at different times or from different positions (Ramirez et al., 2022). The image acquired on August 22, 2024 was selected as the master image.

2.3 Persistent Scatterer Interferometry

Persistent Scatterer Interferometry (PSI) is an InSAR method first proposed by Ferretti et al. (2000) that utilizes amplitude analysis to identify persistent scatterers — making this method more effective in urban areas where man-made establishments and structures have higher reflectivity. In this study, PSI was selected over the SBAS approach due to the specific nature of the areas and assets under observation. Sinkhole formation poses significant risks to lives and property, particularly when it occurs beneath built structures such as homes, schools, and government facilities. As such, these vulnerable and high-impact zones were prioritized as the primary targets of the analysis.

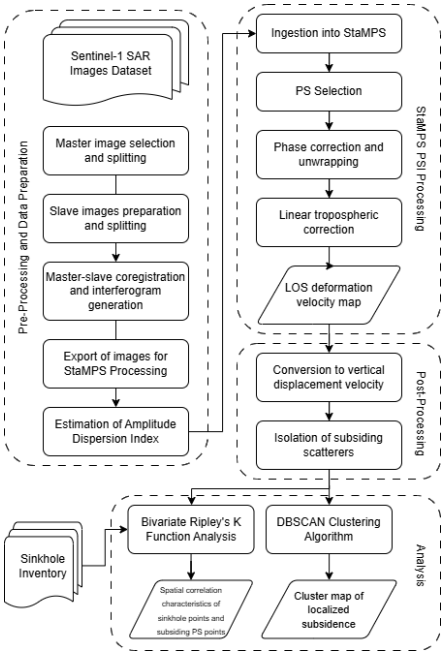

Figure 3. Methodology flowchart for PS-InSAR and post-processing in the study.

The study used the algorithm Stanford Method for Persistent Scatterers (StaMPS), a model developed by Hooper et al. (2004). StaMPS was designed to work on non-urban environments (i.e. volcanic settings) and exploits the spatial correlation of phases to determine stable phase scatterers. Thus, this PS model was determined to be suitable to be applied to a vegetated area such as Guimaras.

The PS-InSAR processing involves the implementation of two main steps: (1) data preparation and pre-processing using SNAP and (2) PSI processing and deformation monitoring using StaMPS. The methodology is detailed in Figure 3.

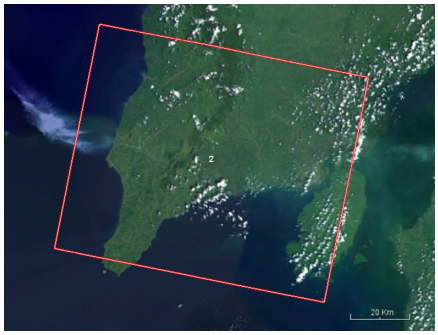

Figure 4. Coverage of SAR image datasets: IW2, Bursts 6-9.

2.3.1 Data Preparation and Pre-Processing: Upon selection of the master image, image splitting was implemented to choose the desired area of interest (AOI). Among the available subswaths, IW2 was selected as it covers the karst landscapes in the western part of Guimaras, including the municipalities of Buenavista, Jordan, and Nueva Valencia, as shown in Figure 4. Bursts 6 to 9 were used to focus on this region.

The slave images underwent image splitting and the subsequent coregistration with the master image. Interferogram generation then followed using back-geocoding with Enhanced Spectral Diversity (ESD), and debursting of the coregistered images was conducted to remove the demarcation pixels. For topographic phase removal, the Shuttle Radar Topography Mission Digital Elevation model (SRTM DEM) 1 arcsec data from the SNAP Library was used.

To properly ingest the dataset into StaMPS for PSI processing, the estimation of the amplitude dispersion index D_A was done. The D_A value, obtained by Equation 1, describes the amplitude stability of the pixel, and is used to select candidate PS points.

$$D_A = \frac{\sigma_A}{\mu_A} \quad (1)$$

where σ_A = standard deviation
μ_A = mean of the amplitude values

The recommended D_A range for StaMPS PSI processing is between 0.40 to 0.42 (Mabaquiao, 2024). Notably, a higher threshold means a higher number of pixels to be retained for phase analysis; the caveat is that noisy pixels are also more likely to be included. To balance this, 0.40 was chosen for the D_A value.

2.3.2 StaMPS PSI Processing: The satellite line-of-sight (LOS) land deformation velocity was calculated using the StaMPS PSI procedure. The pre-processed interferograms were used to select and load the initial PS Candidates (PSCs). Once PSCs are identified, the temporal coherence or the phase noise value for each pixel is then calculated iteratively. Based on the results of this step, final PS candidates were selected. Subsequently, phase unwrapping was conducted, which resolves 2π phase ambiguities to convert wrapped phase values into absolute deformation measurements. Error correction and filtering were then performed, which included the removal of residual orbital and tropospheric signals. The spatially correlated look angle (SCLA) error was estimated and subtracted from the unwrapped phase. The estimation of SCLA and linear tropospheric correction steps were run repeatedly to improve the outputs.

2.4 Post-Processing and Analysis

Conversion to Vertical Displacement Velocity: By combining measurements from SAR images in ascending and descending orbits, LOS land deformation velocities can be decomposed into three dimensions: the horizontal components of the East-West and North-South directions, as well as the vertical component. However, the North-South land deformation is often deemed negligible as per the limitations of Sentinel-1 InSAR with its near-polar orbit radiation (Hu et al., 2014). For studies involving phenomena with dominant vertical displacement—such as landslides and sinkholes—the East-West contribution is further neglected (Qiao et al., 2023). In this study, the vertical displacement values V_u were converted from the descending PSI-derived LOS results using Equation 2. The IW2 subswath used in the data processing has an incidence angle of 39.41°.

$$V_u = \frac{V_{LOS}}{cos\theta} \quad (2)$$

where V_{LOS} = LOS velocity in mm/year
θ = incidence angle of the subswath

2.4.1 Isolation of Subsiding Scatterers: After conversion to vertical displacement values, post-processing was done in order to determine and isolate the "moving scatterers", which was adapted from Oliver-Cabrera et al. (2020). In this case, only negative displacement values were isolated as these denote subsidence, which is indicative of possible sinkhole activity. The PS points were clipped to the Guimaras area, then the summary statistics of displacement values were calculated. Scatterers that have values greater than or equal to 1 standard deviation (1σ) away from the mean displacement value were isolated.

2.4.2 Bivariate Ripley's K Function Analysis: To analyze the spatial relationship between subsiding PS points and sinkhole occurrences, bivariate K-function analysis was implemented on the two point datasets. For each point i, Ripley's K-function calculates the number of points j within a circle with radius r centered on i. $K(r)$ is given by Equation 3:

$$K(r) = \frac{a}{n(n-1)} \sum_{i=1}^{n} \sum_{j=1}^{n} I(d_{ij} \leq r) \quad (3)$$

where a = study region area
n = total number of sinkhole points
d_{ij} = space between point i and point j
$I(d_{ij} \leq r)$ = indicator function that equals 1 when $dij \leq r$ and 0 otherwise

In addition to this, the $K(r)$ function is transformed into the linearized L-function $L(r)$ to ensure stability of the variance as the radius changes. $L(r)$ is defined by Equation 4:

$$L(r) = \sqrt{\frac{K(r)}{\pi}} \quad (4)$$

The bivariate K-function is an extension of the Ripley's K-function; it is capable of detecting spatial patterns between multiple point datasets. This function operates under the null hypothesis of Complete Spatial Randomness (CSR) — an assumption that there is no significant difference between the observed pattern and a random pattern. Moreover, 99 Monte Carlo (MC) simulations were conducted with a 95% confidence interval to establish significance envelopes under CSR. If the observations lie outside the Monte Carlo envelope, the null hypothesis is rejected and a spatial pattern that deviates from randomness exists. The location of the cross-K and cross-L estimates on the graph determines the nature of the spatial relationship between the datasets (Lu et al., 2014).

2.4.3 DBSCAN Clustering Analysis: Sinkholes are localized events; thus, clustering of high density and spatially concentrated subsiding scatterers are necessary to be analyzed for this study. The Density-Based Spatial Clustering Analysis (DBSCAN) was implemented on the isolated subsiding scatterers to determine potential sinkhole-related activity especially in built-up areas. For the DBSCAN parameters, the minimum points in a cluster was set to 5 and the maximum search distance was set to 30 meters. Post-hoc sensitivity analysis of parameters was conducted to ensure robustness of chosen epsilon (maximum neighborhood distance) and minimum points.

3. Results and Discussion

3.1 Ground Deformation Measurements

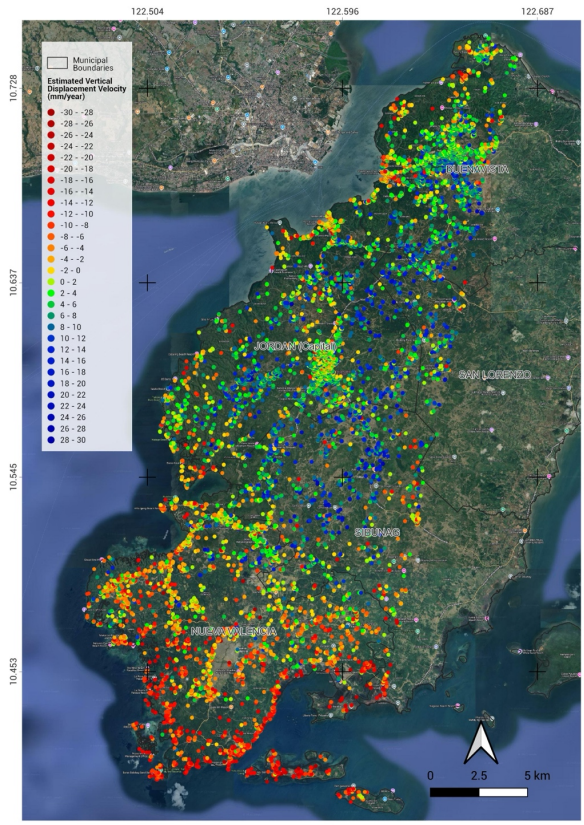

Figure 5. PSI-derived vertical displacement velocity map over the study area.

The StaMPS PSI data processing successfully generated a total of 26,529 Persistent Scatterer (PS) points from the IW2 subswath covering Guimaras Island, as shown in Figure 5. The PS point distribution is heavily concentrated in urban and built-up areas, particularly around town centers, major roads, and infrastructure. This is consistent with the nature of Persistent Scatterer Interferometry (PSI), which favors stable radar reflectors such as buildings, paved surfaces, and other man-made structures. Conversely, vegetated areas and water bodies showed little to no PS coverage, due to temporal decorrelation arising from rapid surface changes between SAR acquisitions (Ramirez et al., 2022).

Upon conversion to vertical displacement velocity values, the color-coded PS velocity map (Figure 5) reveals spatial variations in ground movement across Guimaras. Warm colors (red to orange) indicate negative vertical displacement velocities, which correspond to subsidence or movement away from the satellite. Cool colors (blue to yellow) denote positive velocities, indicating uplift or movement toward the satellite. Green tones signify areas with minimal or negligible movement, interpreted as stable.

The southern municipality of Nueva Valencia exhibited a prominent concentration of subsiding PS points, particularly along the coastal and built-up zones. This area aligns with regions identified by the Mines and Geosciences Bureau (MGB) as highly susceptible to karst subsidence. In contrast, uplift signals were most prevalent in the central parts of the island, particularly around the municipalities of Jordan and Buenavista, while scattered stable PS points were found throughout the study area.

Movement Type	Criteria	No. of Points
Subsiding (significant negative deformation)	≤ –6.125 mm/yr	3,807
Stable (within normal variation)	> –6.125 mm/yr and < +9.675 mm/yr	19,192
Uplifting (significant positive deformation)	≥ +9.675 mm/yr	3,530

Table 1. Classification of points in Guimaras based on vertical displacement velocities relative to mean and standard deviation.

Summary statistics were calculated; the mean displacement velocity across the PS dataset was 1.775 mm/year, with a standard deviation of 7.9 mm/year. To isolate significant subsidence signals, PS points with velocities equal to or exceeding 1σ below the mean (equal to or exceeding –6.125 mm/year) were retained. This threshold yielded a total of 3,807 subsiding scatterers, primarily clustered in Nueva Valencia and southwestern Guimaras. A summary of PS movement classification is shown in Table 1.

3.2 Spatial Correlation Characteristics

The results of the bivariate Ripley's K Analysis (Figure 6) rejected the null hypothesis; the relationship between subsiding scatterers and sinkhole locations exhibit statistically significant clustering. The observation curve lies outside the MC envelope, suggesting significant deviation from CSR. However, the curve lies below the CSR expectation, which indicates spatial repulsion (negative association): the subsiding points are less likely to be near sinkholes than expected under random. Generally, the cross-L and cross-K estimates show that spatial association exists between the datasets, but the sinkhole inventory and subsiding PS points do not coincide spatially.

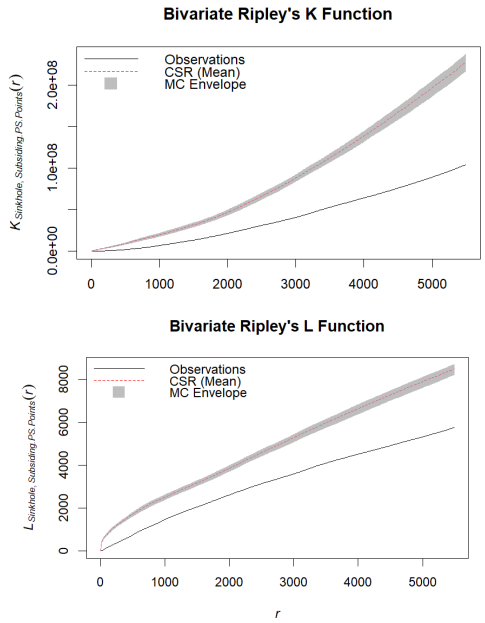

Figure 6. Bivariate K-function analysis results for analyzing spatial relationships between subsiding PS points and sinkhole locations. Red dashed lines indicate expected CSR values and black solid lines denote the observed values. Observations outside the Monte Carlo envelopes (gray area) imply spatial dependence of clustering (above) or repulsion (below).

This contribution has been peer-reviewed. The double-blind peer-review was conducted on the basis of the full paper.
https://doi.org/10.5194/isprs-annals-X-5-W4-2025-43-2026 | © Author(s) 2026. CC BY 4.0 License.

This negative association can be attributed to the nature of PSI. Most of the sinkholes in the inventory are located in vegetated areas, whereas PS points tend to appear in urban areas where persistent scatterers are often located. While PSI provides robust findings on urban subsidence, it is less sensitive in vegetated landscapes which may lead to an apparent mismatch and potential misclassification of subsidence sources. However, deviation from CSR (which can indicate clustering) suggests that PSI can detect areas with localized subsidence or concentrated ground movement, especially in urban areas.

These findings emphasize the importance of in-situ validation to avoid misclassification of localized subsidence as karst-related processes. Aside from sinkholes, other subsiding scatterers could have been caused by other factors such as soil compaction, groundwater withdrawal, slope instability, coastal subsidence, or anthropogenic activities (e.g. mining, quarrying, construction). PSI can thus be a complementary tool for identifying subsidence-related hazards in built-up areas (especially in areas that sinkhole inventories/maps might miss), but ground validation is necessary to verify the actual cause of localized subsidence.

3.3 Clustering Analysis: The findings of the DBSCAN clustering analysis further corroborate the bivariate K-function analysis results regarding spatial clustering. A total of 200 clusters (each with at least five PS points) were identified from the PSI results, shown in Figure 7. The clustering reveals a strong concentration in the southern and southwestern parts of Guimaras, with 158 clusters are located in Nueva Valencia alone. The rest are more sparsely distributed across Jordan (15 clusters), Buenavista (14 clusters), and Sibunag (13 clusters). Notably, no clusters were detected in San Lorenzo, which lies outside the subswath coverage.

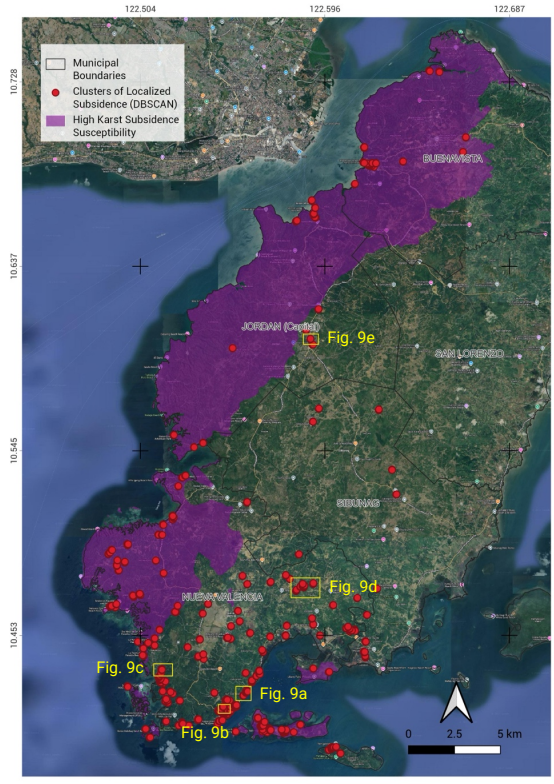

Figure 7. DBSCAN clusters of localized subsidence in Guimaras Island generated from PSI data. Yellow boxes denote specific sites of interest exhibiting significant ground movement.

The karst-prone areas of Nueva Valencia as mapped by MGB contained the largest number of clusters (52), reflecting its geological susceptibility. Interestingly, while karst formations also extend into Jordan and Buenavista, only 9 and 10 clusters were found in those areas, respectively. This may be due to vegetation cover in these northern municipalities, which limits the effectiveness of PSI. Many of the clusters are found along coastal areas, especially in ports, wharfs, and reclaimed zones, and the southern and western coastline of Nueva Valencia.

The clustering algorithm was tested under different values of epsilon and minimum points to test sensitivity to parameter choices. The analysis showed that the number of clusters decreases as both epsilon and minimum points increase, which fall within expectations. Flat segments in the graph show stable clustering across varying epsilon values, but the algorithm is particularly sensitive to the value of minimum points, likely due to point density and distribution. Figure 8 shows that the minPts = 5 stabilizes around ~200 clusters between epsilon = 30m and 60m, indicating that the chosen parameters (5 minimum points, 30m) strike a balance between detecting localized subsidence clusters and avoiding false positives.

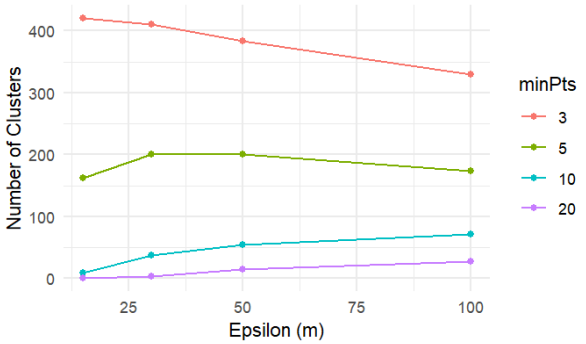

Figure 8. Results of DBSCAN sensitivity analysis. Graph shows variance in clusters as min points and epsilon change.

Five (5) clusters in built-up areas were chosen for detailed inspection (Figure 9), such as coastal barangays like Canhawan and Cabalagnan which recorded displacements of up to –12.94 mm/yr. High-subsidence sites in built up areas include a residential area along the coast of Barangays Cabalagnan and Canhawan (Figure 9a), the area in and around Cabalagnan Elementary School with average displacement velocity of –10.96 mm/yr (Figure 9b), San Roque Day Care Center and the Nueva Valencia Barangay Hall with mean velocity of –10.02 mm/yr (Figure 9c), and Calaya National High School and Calaya Elementary School with mean velocity of –8.85 mm/yr (Figure 9d). A cluster near San Miguel Central School in Jordan also recorded a notable rate of –15 mm/yr (Figure 9e).

Time series deformation graphs from March 2024 to March 2025 were generated for 5 chosen subsiding PS points for each of the areas shown in Figure 9. A general downward trend for the study time period was observed for all sites. Notably, the PS points in Nueva Valencia (Figures 9a to 9d) exhibited similar trends: a sharp downward movement starting from July up to October 2024. Meanwhile, the PS point in Jordan (Figure 9e) showed a steady downward trend all throughout the study time period, except for a steep drop mid-2024. Strong up-and-down fluctuations were observed for all PS points from the end of 2024 continuing to 2025, which can be attributed to anthropogenic activities, although this claim needs further validation. Overall, the steady downward displacement rates for all sites suggest potential subsidence hazards for these built-up areas.

This contribution has been peer-reviewed. The double-blind peer-review was conducted on the basis of the full paper.
https://doi.org/10.5194/isprs-annals-X-5-W4-2025-43-2026 | © Author(s) 2026. CC BY 4.0 License.

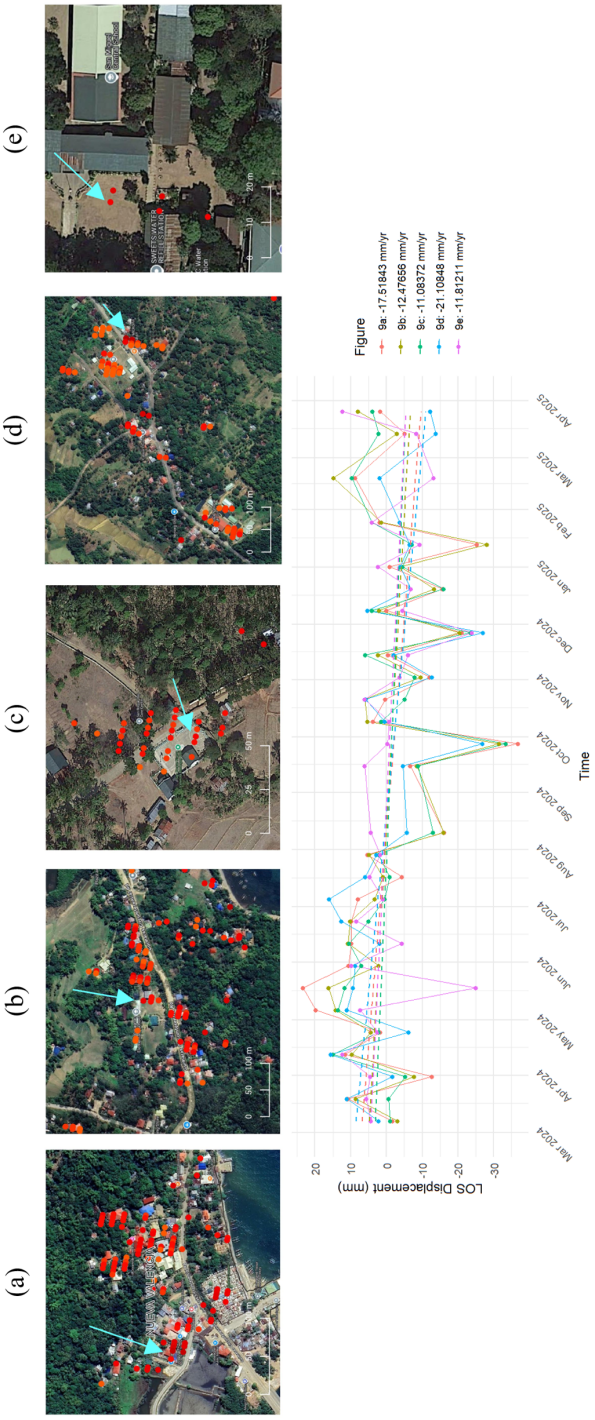

Figure 9. High density clusters of localized subsidence in built up areas: (a) residential area along the coast of Barangays Cabalagnan and Canhawan in Nueva Valencia, (b) Cabalagnan Elementary School, (c) Nueva Valencia barangay hall and San Roque Day Care Center, (d) Calaya National High School and Elementary School, (e) San Miguel Central School in Jordan. Blue arrows point to the scatterers shown in the time series plot. Annual displacement velocity of each PS point is stated in the legend.

4. Conclusions

This study explored the use of Interferometric Synthetic Aperture Radar (InSAR), particularly the Persistent Scatterer Interferometry (PSI) technique, in monitoring ground deformation in the karst landscapes of Guimaras. 3,807 subsiding PS points were identified, primarily concentrated in built-up and urbanized areas.

Bivariate K-function analysis analyzed the spatial correlation and patterns between subsiding PS points and the MGB-derived sinkhole inventory. The findings showed significant deviation from spatial randomness indicating clustering; however, it was determined that subsiding scatterers and sinkhole locations do not coincide with each other.

This suggests that ground deformation, while a useful indicator, should not be interpreted as conclusive evidence of sinkhole activity without further validation. It is therefore concluded that while PSI is limited as a direct sinkhole detection method, it is a useful tool to detect localized subsidence in built-up areas provided that the necessary ground validation is performed.

Clustering analysis revealed that most deformation activity was concentrated in the southern municipalities, with Nueva Valencia accounting for 79% of the identified clusters. Several clusters corresponded with critical infrastructure and public buildings, such as schools and government facilities, where average vertical subsidence velocities reached as high as –36 mm/yr. Although Buenavista and Jordan also contain significant areas of karst terrain, the number of clusters detected in these municipalities was notably lower. This disparity is not necessarily indicative of lower subsidence risk; rather, it highlights a limitation of the PSI method in vegetated areas. The presence of dense vegetation, common in the karst zones of Jordan and Buenavista, can lead to underrepresentation of subsidence.

Recommendations for future studies include exploration of methods better suited to vegetated environments, such as SBAS-InSAR or LiDAR-based terrain analysis, for more comprehensive results in the study area. Another recommendation of note is that ground validation be implemented alongside remote sensing techniques for sinkhole detection to distinguish between karst-related subsidence and other types of ground instability. The authors also recommend the use of elevation data from GNSS stations to provide calibrated and ground-truthed deformation measurements to obtain the actual displacement on the ground is imperative, as the results derived from StaMPS PSI are relative velocities. Furthermore, other factors that influence subsidence, such as urban development, infrastructure loading, soil compaction, groundwater drawdown, and coastal dynamics, can also be studied further.

Based on the findings of this study, the municipality of Nueva Valencia should be prioritized in terms of ground stability monitoring and disaster preparedness planning, given its high concentration of deformation clusters, especially in built-up and karst-prone coastal areas. The findings of this study can help supplement the knowledge of local government units regarding the potential risks posed by natural karst processes and develop early warning systems that integrate satellite-based monitoring with on-the-ground risk assessments.

Acknowledgements

This research was done as part of the Modern Geospatial and Collaborative Solutions for the Development of Smart Regions (SMART METRO) Project, implemented by the University of the Philippines Training Center for Applied Geodesy and Photogrammetry (TCAGP), with support from the Department of Science and Technology (DOST) and the Philippine Council for

Industry, Energy, and Emerging Technology Research and (a) (b) (c) (d) (e) Development (PCIEERD), under Project No. 1212042. The authors also acknowledge the Province of Guimaras, particularly the municipal planning and DRRM offices of Jordan, Buenavista, and Nueva Valencia, for providing the datasets used in this study.

References

Bagheri-Gavkosh, M., Hosseini, S. M., Ataie-Ashtiani, B., Sohani, Y., Ebrahimian, H., Morovat, F., & Ashrafi, S., 2021. Land subsidence: A global challenge. *Science of The Total Environment*, 77. doi.org/10.1016/J.SCITOTENV.2021.146193.

Even, M., & Schulz, K., 2018. InSAR Deformation Analysis with Distributed Scatterers: A Review Complemented by New Advances. *Remote Sensing*, 10(5), 744. doi.org/10.3390/RS10050744.

Ferretti, A., Prati, C., & Rocca, F., 2000. Nonlinear subsidence rate estimation using permanent scatterers in differential SAR interferometry. *IEEE Transactions on Geoscience and Remote Sensing*, *38*(5 I), 2202–2212. doi.org/10.1109/36.868878.

Galloway, D. L., & Burbey, T. J., 2011. Review: Regional land subsidence accompanying groundwater extraction. *Hydrogeology Journal*, 19(8), 1459–1486. doi.org/10.1007/S10040-011-0775-5/FIGURES/4.

Hu, J., Li, Z. W., Ding, X. L., Zhu, J. J., Zhang, L., & Sun, Q., 2014. Resolving three-dimensional surface displacements from InSAR measurements: A review. *Earth-Science Reviews*, 133, 1–17. doi.org/10.1016/J.EARSCIREV.2014.02.005.

Institute for Global Environmental Strategies (IGES), & Partnerships in Environmental Management for the Seas of East Asia (PEMSEA)., 2022. Achieving Coastal Resilience Through Local Knowledge-Based Adaptation Planning: A Pilot Project in Guimaras Province, Philippines Workshop Report. pemsea.org (16 January 2025).

Kulshrestha, A. (2023). InSAR Time Series Analysis for Sinkhole Detection using Deep Learning. research.utwente.nl (7 January 2025).

Llanes, F., Galang, J. A., Rabonza, M., Ferrer, P. K., Lagmay, A., Eco, N., Cuadra, C., Suarez, K., & Dasallas, L., 2018. Geohazards Assessment. Disaster Risk Reduction and Management Handbook for Academic Institutions, 55–104. University of the Philippines Press.

Lu, P., Bai, S., & Casagli, N., 2014. Investigating Spatial Patterns of Persistent Scatterer Interferometry Point Targets and Landslide Occurrences in the Arno River Basin. *Remote Sensing 2014*, 6(8), 6817–6843. doi.org/10.3390/RS6086817.

Mabaquiao, L. C., 2024. Performance Evaluation Of Temporal Model And Spatial Correlation Methods For Persistent Scatterer Determination In Landslide Prone Areas. *International Archives of the Photogrammetry, Remote Sensing and Spatial Information Sciences - ISPRS Archives*, *48*(4/W8-2023), 343–349. doi.org/10.5194/ISPRS-ARCHIVES-XLVIII-4-W8-2023-343-2024.

Malinowska, A. A., Witkowski, W. T., Hejmanowski, R., Chang, L., van Leijen, F. J., & Hanssen, R. F., 2019. Sinkhole occurrence monitoring over shallow abandoned coal mines with satellite-based persistent scatterer interferometry. *Engineering Geology*, *262*. doi.org/10.1016/J.ENGGEO.2019.105336.

Matus, C., 2013. 100 Sinkholes Found in Bohol after Quake. *Philippine Daily Inquirer*. newsinfo.inquirer.net/519051/100-sinkholes-found-in-bohol-after-quake (17 January 2025).

Mines and Geosciences Bureau Regional Office No. 6, 2018. *Year-End Report 2018*. mgb6.org (16 January 2025).

Nam, B. H., Choi, S., Copeland, T., & Kim, Y. J., 2023. Social Vulnerability and Geohazards: Review and Implications. *Advances in Natural and Technological Hazards Research*, 51, 3–37. doi.org/10.1007/978-3-031-24541-1_1.

Oliver-Cabrera, T., Wdowinski, S., Kruse, S., & Robinson, T., 2020. InSAR Detection of Localized Subsidence Induced by Sinkhole Activity in Suburban West-Central Florida. *IAHS*, 382, 155–159. doi.org/10.5194/piahs-382-155-2020.

Orhan, O., Haghshenas Haghighi, M., Demir, V., Gökkaya, E., Gutiérrez, F., & Al-Halbouni, D., 2023. Spatial and Temporal Patterns of Land Subsidence and Sinkhole Occurrence in the Konya Endorheic Basin, Turkey. *Geosciences, 14*(1), 5. doi.org/10.3390/GEOSCIENCES14010005.

Peng, L., & Tan, J., 2023. Identifying Neighborhood Effects on Geohazard Adaptation in Mountainous Rural Areas of China: A Spatial Econometric Model. *International Journal of Disaster Risk Science*, *14*(6), 919–931. doi.org/10.1007/S13753-023-00523-9/TABLES/3.

Province of Guimaras, 2019. Province of Guimaras: Environmental Profile. guimaras.gov.ph (7 January 2025).

Qiao, X., Chu, T., Tissot, P., & Holland, S., 2023. Sentinel-1 InSAR-derived land subsidence assessment along the Texas Gulf Coast. *International Journal of Applied Earth Observation and Geoinformation*, 125, 103544. doi.org/10.1016/J.JAG.2023.103544.

Ramirez, R. A., Abdullah, R. E. E., & Rubio, C. J. P., 2022. S1-PSINSAR MONITORING AND HYPERBOLIC MODELING OF NONLINEAR GROUND SUBSIDENCE IN NAGA CITY, CEBU ISLAND IN THE PHILIPPINES. *GEOMATE Journal*, *23*(100), 102–109. doi.org/10.21660/2022.100.g12121.

Richardson, S., 2013. Sinkhole and subsidence record in the Chuniespoort group dolomite, Gauteng, South Africa, University of Pretoria, Pretoria. hdl.handle.net/2263/33182 (25 January 2025).

Sulapas, J. J. S., Ybañez, A. A. B., Marasigan, K. M. M., Grageda, J. M. B. M., & Lagmay, A. M. F. A., 2024. Ground subsidence in major Philippine metropolitan cities from 2014 to 2020. *International Journal of Applied Earth Observation and Geoinformation*, 133, 104107. doi.org/10.1016/J.JAG.2024.104107.

Theron, A., & Engelbrecht, J., 2018. The Role of Earth Observation, with a Focus on SAR Interferometry, for Sinkhole Hazard Assessment. *Remote Sensing*, 10(10), 1506. doi.org/10.3390/RS10101506.

Wu, P. C., Wei, M., & D'Hondt, S., 2022. Subsidence in Coastal Cities Throughout the World Observed by InSAR. *Geophysical Research Letters*, 49(7). doi.org/10.1029/2022GL098477.